Atmospheric
Chemistry
and Physics

Nitrate formation from heterogeneous uptake of dinitrogen pentoxide during a severe winter haze in southern China

Hui Yun[1], **Weihao Wang**[1], **Tao Wang**[1], **Men Xia**[1], **Chuan Yu**[1,2], **Zhe Wang**[1], **Steven C. N. Poon**[1], **Dingli Yue**[3], and **Yan Zhou**[3]

[1]Department of Civil and Environmental Engineering, The Hong Kong Polytechnic University, Hong Kong, China
[2]Environment Research Institute, Shandong University, Jinan, China
[3]Guangdong Environmental Monitoring Center, State Environmental Protection Key Laboratory
of Regional Air Quality Monitoring, Guangzhou, China
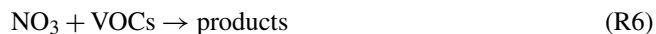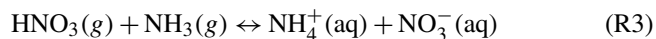
Correspondence: Tao Wang (cetwang@polyu.edu.hk)

Abstract. Nitrate (NO_3^-) has become a major component of fine particulate matter ($PM_{2.5}$) during hazy days in China. However, the role of the heterogeneous reactions of dinitrogen pentoxide (N_2O_5) in nitrate formation is not well constrained. In January 2017, a severe haze event occurred in the Pearl River Delta (PRD) of southern China during which high levels of $PM_{2.5}$ ($\sim 400\,\mu g\,m^{-3}$) and O_3 ($\sim 160\,ppbv$) were observed at a semi-rural site (Heshan) in the western PRD. Nitrate concentrations reached $108\,\mu g\,m^{-3}$ (1 h time resolution), and the contribution of nitrate to $PM_{2.5}$ was nearly 40 %. Concurrent increases in NO_3^- and $ClNO_2$ (with a maximum value of 8.3 ppbv at a 1 min time resolution) were observed in the first several hours after sunset, indicating an intense N_2O_5 heterogeneous uptake by aerosols. The formation potential of NO_3^- via N_2O_5 heterogeneous reactions was estimated to be between 29.0 and 77.3 $\mu g\,m^{-3}$ in the early hours (2 to 6 h) after sunset based on the measurement data, which could completely explain the measured increase in the NO_3^- concentration during the same time period. Daytime production of nitric acid from the gas-phase reaction of $OH + NO_2$ was calculated with a chemical box model built using the Master Chemical Mechanism (MCM v3.3.1) and constrained by the measurement data. The integrated nocturnal nitrate formed via N_2O_5 chemistry was comparable to or even higher than the nitric acid formed during the day. This study confirms that N_2O_5 heterogeneous chemistry was a significant source of aerosol nitrate during hazy days in southern China.

1 Introduction

Severe haze in China has been a major concern of the regulatory and scientific communities in recent years. Nitrate has also been identified as an important component of $PM_{2.5}$ during hazy days in both summer and winter (e.g., Huang et al., 2014; Li et al., 2018; Pathak et al., 2009; Zhang et al., 2015). Moreover, the proportion of nitrate in $PM_{2.5}$ has steadily increased over the last decade due to the lagged control of NO_x emissions compared to SO_2 (Fu et al., 2014; Geng et al., 2017; Qu et al., 2017; Reuter et al., 2014; X. Wang et al., 2016). As a result, the concentrations of nitrate in $PM_{2.5}$ / $PM_{1.0}$ have been even higher than those of sulfate during some haze events (Ge et al., 2017; Li et al., 2017; Liu et al., 2015; Yang et al., 2017; Yue et al., 2015).

Nitrate is formed from NO_x during both the daytime and nighttime. During the day, nitric acid (HNO_3) is produced through the gas-phase reaction between OH and NO_2 (Reaction R1), while this pathway is insignificant at night due to very low OH concentrations (e.g., Seinfeld and Pandis, 2016). Nitric acid can react with ammonia (NH_3) to form ammonium nitrate (NH_4NO_3), and an equilibrium can be reached for these three compounds between the gas phase and the particle phase (Reactions R2, R3). During nighttime, the heterogeneous uptake of N_2O_5, which is formed from reactions involving O_3, NO_2, and NO_3, becomes a source of nitrate and also produces gaseous $ClNO_2$ when chloride-containing aerosol is present (Reactions R4–R7; Finlayson-Pitts et al., 1989). This nitrate formation pathway is only important at night due to the fast photolysis of NO_3 during the

day. Compared to the relatively well-understood formation of aerosol nitrate via the $OH + NO_2$ reaction, the contribution from N_2O_5 heterogeneous reactions has been poorly quantified due to the limited knowledge of key factors controlling the heterogeneous processes, such as the N_2O_5 uptake coefficient ($\gamma_{N_2O_5}$) and $ClNO_2$ yield (ϕ_{ClNO_2}) (Brown and Stutz, 2012; Chang et al., 2011).

$$OH + NO_2 + M \rightarrow HNO_3 + M \tag{R1}$$
$$HNO_3(g) + NH_3(g) \leftrightarrow NH_4NO_3(s) \tag{R2}$$
$$HNO_3(g) + NH_3(g) \leftrightarrow NH_4^+(aq) + NO_3^-(aq) \tag{R3}$$
$$NO_2 + O_3 \rightarrow NO_3 \tag{R4}$$
$$NO_2 + NO_3 + M \leftrightarrow N_2O_5 + M \tag{R5}$$
$$NO_3 + VOCs \rightarrow products \tag{R6}$$
$$N_2O_5 + H_2O \text{ or } Cl^-(aq)$$
$$\rightarrow (2 - \phi)NO_3^-(aq) + \phi ClNO_2(g) \tag{R7}$$

Model studies initially treated $\gamma_{N_2O_5}$ as a constant (0.03 to 0.1) (Dentener and Crutzen, 1993; Makar et al., 1998; Munger et al., 1998; Schaap et al., 2004; Wen et al., 2015; Xue et al., 2014), and later utilized several parameterization schemes of $\gamma_{N_2O_5}$ and ϕ_{ClNO_2} based on laboratory investigations of their dependence on aerosol composition and aerosol water content (Anttila et al., 2006; Bertram and Thornton, 2009; Davis et al., 2008; Evans and Jacob, 2005; Riemer et al., 2003, 2009; Roberts et al., 2009). However, recent studies have found a significant discrepancy between the field-derived and the parameterized $\gamma_{N_2O_5}$ and ϕ_{ClNO_2} (McDuffie et al., 2018; Phillips et al., 2016; Tham et al., 2018; X. Wang et al., 2017; Z. Wang et al., 2017; Zhou et al., 2018). These findings suggest that N_2O_5 uptake is more complicated than previously thought, and a better understanding of the uptake process is needed to improve the prediction of nitrate and haze.

In addition to the modeling approach, field measurements of trace gases and aerosol composition have been used to infer the contribution of N_2O_5 heterogeneous chemistry to nitrate formation. Pathak et al. (2009) postulated the importance of N_2O_5 heterogeneous reactions with respect to the high aerosol nitrate observed in Beijing and Shanghai in summertime by examining the variation of nitrate with the change in relative humidity (RH) and the equilibrium between anions and cations in $PM_{2.5}$. Pathak et al. (2011) further investigated nitrate formation using a coupled aqueous phase radical mechanism (CAPRAM) and a gas-phase chemistry mechanism (RACM, without $ClNO_2$ chemistry). By constraining the uptake coefficient of N_2O_5 in the range from 0.001 to 0.1, they reproduced the observed enhancement of nitrate and suggested that N_2O_5 uptake by aerosols contributed to 50 % to 100 % of the nighttime increase in nitrate. A similar method was recently used by Wen et al. (2018) to simulate the summertime nitrate formation in the North China Plain (NCP), which demonstrated the dominant contribution of N_2O_5 heterogeneous reactions to night-

time nitrate formation. Based on the observed covariation of nitrate and RH, Wang et al. (2009) speculated that N_2O_5 reactions dominated the nitrate formation on polluted days with high NO_2 and O_3 concentrations in Shanghai. Neither N_2O_5 nor $ClNO_2$ was measured during these early observation-based studies. A recent study (H. Wang et al., 2017) inferred $\gamma_{N_2O_5}$ from the measured N_2O_5 on 4 days in urban Beijing and estimated the lower limit of the formation potential of aerosol nitrate assuming a unity ϕ_{ClNO2} because $ClNO_2$ was not measured. Their result showed a comparable contribution to nitrate formation from the N_2O_5 heterogeneous chemistry and from the daytime pathway of the $OH + NO_2$ reaction.

In the present study, N_2O_5, $ClNO_2$, and the related chemical and meteorological parameters were measured at a semi-rural site in the Pearl River Delta of southern China from 2 to 15 January 2017. A severe haze event was observed during the field study with $PM_{2.5}$ reaching $400\,\mu g\,m^{-3}$ and O_3 peaking at 160 ppbv. $ClNO_2$, which is only known to be produced from N_2O_5 heterogeneous uptake, reached 8.3 ppbv, which is the largest reported value to date and revealed extremely active N_2O_5 chemistry during the abovementioned episode. The concurrent measurements of N_2O_5, $ClNO_2$, and aerosol nitrate provide better constraints for elucidating nighttime NO_3 / N_2O_5 chemistry and aerosol nitrate formation. An overview of the measurement data was first presented. The nighttime processes that led to the formation of nitrate (e.g., the production of NO_3 and N_2O_5, N_2O_5 uptake coefficient, and $ClNO_2$ yield) were analyzed. The nighttime formation potential of nitrate was estimated based on these data and compared to the measured increase in nitrate. The daytime production of nitric acid via the $OH + NO_2$ reaction was calculated based on a box model using the Master Chemical Mechanism (MCM v3.3.1) and compared to the nighttime formation potential of nitrate.

2 Methods

2.1 Site description

The field observation was conducted at the Guangdong atmospheric supersite, a semi-rural site located at Hua Guo Shan (HGS, 22.728° N, 112.929° E) southwest of the city of Heshan from 2 to 15 January 2017. As shown in Fig. 1, HGS is a hill with a height of 60 m a.s.l. All measurement instruments were located on the fourth floor of a four-story building on the top of the hill. The observation site was located in the western PRD where the economic activity and population density are much lower than the central PRD. There are five main roads near the HGS site, including three national roads (G325, G94, and G15), and two provincial roads (S272 and S270). The hill is covered by subtropical trees and surrounded by similar hills within close proximity; a few residents live at the foot of the hill, and there is some farmland in the area.
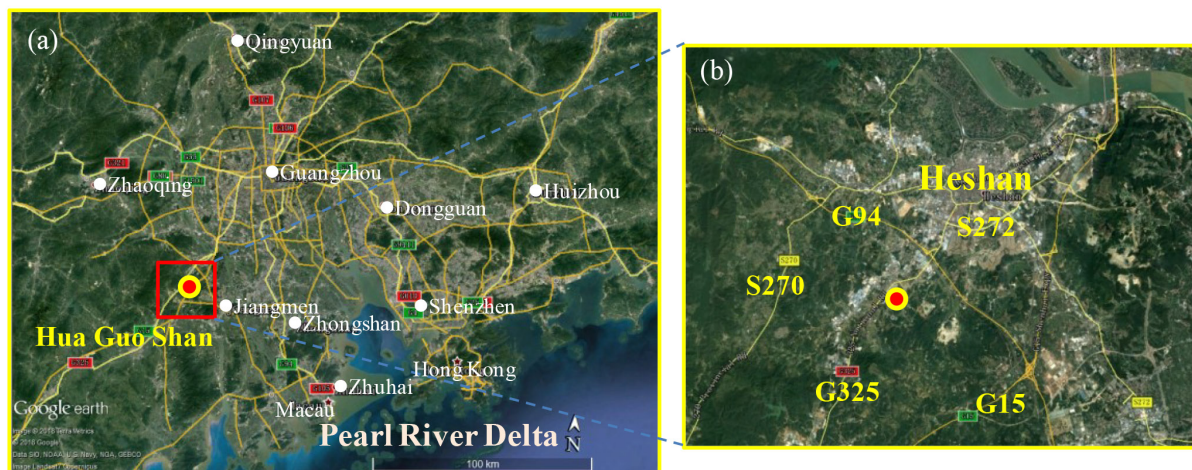
Figure 1. (a) Google map images of the Pearl River Delta in Guangdong Province and the measurement site (Hua Guo Shan). **(b)** The topography and major roads (shown by number) adjacent to the measurement site.

2.2 Chemical ionization mass spectrometer

N_2O_5 and $ClNO_2$ were simultaneously observed using a quadrupole chemical ionization mass spectrometer (CIMS, THS Instruments, Atlanta). The same instrument had been used in several previous studies in southern and northern China (Tham et al., 2016; T. Wang et al., 2016; Z. Wang et al., 2017). The reader can refer to these earlier papers for a detailed description of the measurement principle, calibration, and maintenance procedures. Briefly, ambient N_2O_5 and $ClNO_2$ are converted to ion clusters of $I(N_2O_5)^-$ and $I(ClNO_2)^-$ by Iodide ions (I^-) that are produced by exposing CH_3I/N_2 ($0.3\% \ v/v$) to an alpha radioactive source, 210-Po, and are subsequently detected at 235 and $208 \, m \, z^{-1}$, respectively. Activated carbon packed in a filter was used to determine the instrument background, which were 10.2 ± 2.2 and $8.9 \pm 2.0 \, Hz$ on average for N_2O_5 and $ClNO_2$, respectively. In situ offline calibration was carried out every day for N_2O_5 and every 2 days for $ClNO_2$ by mixing the respective synthetic standard into humidified zero air (with RH controlled at 60 % in the present study). The N_2O_5 standard was generated by reacting excess NO_2 with O_3 and determined from the decrease of NO_2, and the $ClNO_2$ was synthesized by the uptake of a known concentration of N_2O_5 on a NaCl slurry (see T. Wang et al., 2016 and Tham et al., 2016 for details). The average sensitivity of N_2O_5 and $ClNO_2$ was 0.9 ± 0.3 and $0.7 \pm 0.2 \, Hz \, pptv^{-1}$, respectively. The dependence of the sensitivity on the relative humidity was measured during the field study (see Fig. S1) and was used to correct for the RH effect based on the measured ambient RH values. The detection limits of N_2O_5 and $ClNO_2$ were both $6 \, pptv$ (2σ, 1 min-averaged data).

The inlet of the CIMS instrument was set approximately 1.5 m above the roof with 6 m long PFA-Teflon tubing as the sampling line. The total sampling flow was set as 11 standard liters per minute (SLPM). Four SLPM were diverted into the CIMS, the O_3 analyzer, and NO_x analyzer, and the remaining part was evacuated directly from the system. The total residence time was less than 1 s in the sampling system. Following our previous practice, the inlet tubing and fittings were replaced every afternoon and washed in an ultrasonic bath to reduce the influence of particle deposition on the tubing wall. The loss of N_2O_5 on the tubing wall was checked on site by injecting N_2O_5 into the ambient air before and after the tubing replacement; the loss was found to be around 10 % in the "clean" tubing and nearly 40 % by the next afternoon. Because our analysis mainly focused on data from the first few hours of evening, the loss was insignificant and thus was not corrected in our final data. However, this bias could be important in the later period before tube replacement. The uncertainty of the measurement was estimated to be $\pm 25\%$ for both N_2O_5 and $ClNO_2$ (T. Wang et al., 2016). The time resolution for the measurement was approximately 10 s, and the derived data were later averaged to a time resolution of 1 min for further analysis.

2.3 Other measurements

Trace gases of CO, SO_2, O_3, NO_x, total reactive nitrogen (NO_y), nitrous acid (HONO), C2 to C10 non-methane hydrocarbons (NMHCs), oxygenated hydrocarbons (OVOCs), and aerosol chemical composition and number concentrations were also measured. Table 1 summarizes the principle, detection limit and uncertainty of the measuring instruments.

CO was observed using a gas filter correlation analyzer (Thermo Scientific, Model 48i). SO_2 was measured using a pulsed fluorescence analyzer (Thermo Scientific, Model 43i). O_3 was determined using a UV photometric analyzer (Thermo Scientific, Model 49i). NO and NO_2 were detected with a chemiluminescence instrument (Thermo Sci-

Table 1. Technique, limit of detection, and uncertainty of measuring instruments for trace gases and aerosols.

Species	Measurement techniques	Uncertainty	Detection limits
$ClNO_2$, N_2O_5	CIMS	$\pm 25\%$	6 pptv
HONO	LOPAP	$\pm 20\%$	7 pptv
O_3	UV photometry	$\pm 5\%$	0.5 ppbv
NO	Chemiluminescence	$\pm 20\%$	0.06 ppbv
NO_2	Photolytical converter and chemiluminescence	$\pm 20\%$	0.3 ppbv
NO_y	MoO catalytic converter and chemiluminescence	$\pm 5\%$	<0.1 ppbv
SO_2	Pulsed-UV fluorescence	$\pm 5\%$	0.1 ppbv
CO	IR photometry	$\pm 5\%$	4 ppbv
NMHCs	GC-FID/MS	$\pm 15\%$–20%	20–300 pptv
OVOCs	DNPH-HPLC	$\pm 1\%$–15%	20–450 pptv
$PM_{2.5}$	MAAP	$\pm 10\%$	$<0.1\,\mu g\,m^{-3}$
Aerosol ions	GAC-IC	$\pm 10\%$	0.01–$0.16\,\mu g\,m^{-3}$
OC / EC	RT-4 SUNSET	$\pm 4\%$–6%	$0.2\,\mu g\,cm^{-2}$

entific, Model 42i) with a photolytic converter to convert NO_2 to NO (Xu et al., 2013). NO_y was determined using a chemiluminescence analyzer which was equipped with a molybdenum oxide (MoO) catalytic converter (Thermo Scientific, Model 42i-Y). HONO was detected using a long path absorption photometer (QUMA, Model LOPAP-03) (Xu et al., 2015). NMHCs were determined using an online gas chromatograph (GC) coupled with a flame ionization detector (FID) and a mass spectrometer (MS) (Wang et al., 2014). NMHCs were only measured from 2 to 8 January 2017 due to the maintenance of the GCMS after 8 January. OVOCs (e.g., formaldehyde, acetaldehyde, acetone, and methyl ethyl ketone) were sampled using 2,4-dinitrophenylhydrazine (DNPH) cartridges every 3 h and were later analyzed with a high-performance liquid chromatography (HPLC) system (Cui et al., 2016).

Concentrations of $PM_{2.5}$ were detected with a multi-angle absorption photometer (MAAP; Thermo Scientific, Model 5012). The ionic compositions of $PM_{2.5}$ were measured with an ion chromatography (GAC-IC) system equipped with a gas and aerosol collector at a time resolution of 30 min (Dong et al., 2012), and the data were also averaged every 1 h to meet the time resolution of other components of $PM_{2.5}$. Organic carbon (OC) and elemental carbon (EC) were measured using an online OC / EC analyzer (RT-4, SUNSET) with a time resolution of 1 h (Bauer et al., 2009). A scanning mobility particle sizer (SMPS Model 3936L75, TSI) was used to determine the dry-state particle number size distribution, covering the size range from 16.5 to 1000 nm. The ambient (wet) particle number size distributions were estimated based on a size-resolved kappa-Köhler function considering the variation with relative humidity (Hennig et al., 2005; Liu et al., 2014). In the present study, data with a RH greater than 90 % were excluded due to the large uncertainty of the growth factor at very high RH. The aerosol surface area density was then derived using the ambient particle number size distribution (wet) and an assumption of spherical particles with an estimated uncertainty of around 30 % (Tham et al., 2016; Z. Wang et al., 2017).

Meteorological parameters were measured with a portable weather station (WXT520, Vaisala, Finland), including temperature, relative humidity (RH), wind direction, wind speed, and pressure. A pyranometer (CMP22, Kipp & Zonen B.V., Holland) was used to measure the solar radiation, and the data were then utilized to derive the photolysis frequency of NO_2 based on the method of Trebs et al. (2009).

2.4 Chemical box model

To estimate the daytime formation of nitric acid via the reaction of $OH + NO_2$, an observation-based chemical box model developed with the latest version of the MCM (v3.3.1) (Jenkin et al., 2003, 2015; Saunders et al., 2003) and an updated chlorine (Cl) radical chemistry module (Xue et al., 2015) was utilized to estimate the mixing ratio of OH radicals and the reaction rate of $OH + NO_2$. The integrated production of nitric acid during daytime was then calculated based on the simulation results. The box model was constrained with the observation data every 10 min, including the data relating to N_2O_5, $ClNO_2$, HONO, O_3, NO, NO_2, SO_2, CO, C2 to C10 NMHCs, OVOCs (formaldehyde, acetaldehyde, acetone, and MEK), temperature, aerosol surface area density, and $J(NO_2)$, which were first averaged or interpolated. Average concentrations of NMHC species during the day (07:00 to 17:00) and at night (17:00 to 07:00 of the next day) are shown in Table S1. A function considering the variation of the solar zenith angle (Saunders et al., 2003) was used to calculate the photolysis frequencies of HONO, O_3, and other species in clear sky, which were then corrected with the $J(NO_2)$ values in the real environment. The $J(ClNO_2)$

was treated the same as in Tham et al. (2016). The lifetime of unconstrained species with respect to the physical loss was set as 8 h in a boundary layer with a depth of 1000 m (equivalent to $3.47 \times 10^{-5}\,\text{s}^{-1}$) in order to avoid their accumulation. The model was run from 00:00 on 3 January to 11:00 on 8 January 2017. To stabilize the intermediate species, the simulation for the first 24 h was repeated six times. Sensitivity tests were carried out by reducing the input concentrations by 10 % to check the deviation of the average daytime (07:00–17:00) rate of the $OH + NO_2$ reaction. The simulated rate of the $OH + NO_2$ reaction was most sensitive to HONO, followed by NO_x and OVOCs (see Sect. S1 and Fig. S2 in the Supplement).

3 Results and discussion

3.1 Overview of the observation

Figure 2 shows the time series of N_2O_5, $ClNO_2$, components of $PM_{2.5}$, and related trace gases and meteorological parameters from 18:40 on 2 January to 11:00 on 15 January 2017. The average temperature and RH values during the measurement period were $17 \pm 4\,°\text{C}$ and $86 \pm 14\,\%$, respectively. A severe pollution episode occurred from 3 to 7 January due to stagnant meteorological conditions (Fig. 3a), and the concentrations of most pollutants decreased to very low levels on 9 January and from 12 to 15 January, which corresponded to the change in weather conditions. The most polluted days were 5 and 6 January with the highest $PM_{2.5}$ value of $400\,\mu\text{g}\,\text{m}^{-3}$ and the highest O_3 concentration of 160 ppbv. The $PM_{2.5}$ data from the PRD regional air quality monitoring network revealed that the HGS site was within the most polluted area during this haze event (Fig. 3b). This pollution event was characterized by concurrent high levels of $PM_{2.5}$ and O_3 and was in contrast to the winter haze in north China, which experienced high $PM_{2.5}$ values but low O_3 concentrations (e.g., Sun et al., 2016; H. Wang et al., 2018a). The mixing ratios of N_2O_5 and $ClNO_2$ were up to 3358 and 8324 pptv (1 min time resolution), respectively, indicating active N_2O_5 heterogeneous chemistry.

Very high concentrations of aerosol nitrate (up to $108\,\mu\text{g}\,\text{m}^{-3}$; 1 h time resolution) were also observed during the multi-day episode. Nitrate contributed to 24 % of the total $PM_{2.5}$ mass concentration on average, which was comparable to that of organic matter ($OM = 1.7 \cdot OC$, 28 %) and much higher than that of sulfate (16 %) and ammonium (11 %). The contribution of nitrate to the $PM_{2.5}$ increased with an increase in the nitrate concentration, and reached nearly 40 % at its peak, indicating that nitrate was a dominant component of the $PM_{2.5}$ on the most polluted days. The concentration of NO_3^- exhibited a concurrent increase with that of $ClNO_2$ in the early nighttime from 3 to 4, 4 to 5, 5 to 6, and 9 to 10 January (see Fig. 4), suggesting that N_2O_5 heterogeneous reactions significantly contributed to the formation of

nitrate during the night. The measured increases of the NO_3^- concentration during these four nights were 17.1, 50.9, 43.3, and $32.7\,\mu\text{g}\,\text{m}^{-3}$, respectively. A similar increase in $ClNO_2$ was observed from 6 to 7 January, but the composition of the $PM_{2.5}$ was not available due to instrument maintenance. Apart from chemical reactions, the evolution of the planetary boundary layer (PBL) also affects the concentrations of trace gas and aerosols. The height of PBL generally decreases after sunset due to the fast decrease in the land temperature, which can lead to the accumulation of primary pollutants (and secondary pollutants) at the surface if significant local sources are present. For example, on the night from 4 to 5 January (see Fig. 5), the CO and NO_y levels increased between 18:00 and 19:00 LT with the enhancement of $ClNO_2$ and nitrate, indicative of an accumulation of primary emissions; however, after this period of time the primary pollutants decreased for 3 h while $ClNO_2$ and nitrate continued to increase due to the nighttime chemical process.

In the remainder of this paper, we will focus on the detailed analysis of the abovementioned five nights to investigate the role of N_2O_5 heterogeneous chemistry in nitrate formation.

3.2 N_2O_5 heterogeneous chemistry on the selected nights

3.2.1 Production of NO_3 and N_2O_5

The first step in the nighttime nitrate formation via N_2O_5 chemistry is the production of NO_3 and N_2O_5. To gain insight into the key factors affecting the NO_3 / N_2O_5 chemistry, the variation of N_2O_5 and the production rate of NO_3 were examined in relation to some relevant gases and meteorological parameters on the selected five nights. Figure 5 shows the data for the night from 4 to 5 January as an example. Some common features were identified for all five nights. In general, low wind speed ($<2.0\,\text{m}\,\text{s}^{-1}$) at night facilitated the accumulation of air pollutants, and high RH was favorable for N_2O_5 heterogeneous uptake. In addition, high aerosol surface area density provided interfaces for N_2O_5 heterogeneous reactions.

In the first couple of hours after sunset (Fig. 5, red rectangle), N_2O_5 exhibited a peak and then quickly dropped to hundreds of pptv, while nitrate and $ClNO_2$ concurrently increased, which was indicative of the local production and loss of N_2O_5. NO was below the detection limit during this period. The production rates of NO_3 ($P_{NO_3} = k_{NO_2 + O_3}[NO_2][O_3]$) were the fastest just after sunset and decreased gradually due to reduced O_3 levels. There was a period later in the night (22:00 to 01:00) when fresh emissions of NO were observed, and the production of NO_3 was suppressed due to the titration of O_3 by NO. In the later nighttime, NO was below the detection limit (Fig. 5, blue rectangle). During this period, NO_3 and N_2O_5 were produced at moderate rates, and the very low N_2O_5 concentrations (below the detection limit) suggested a fast loss of N_2O_5 prob-
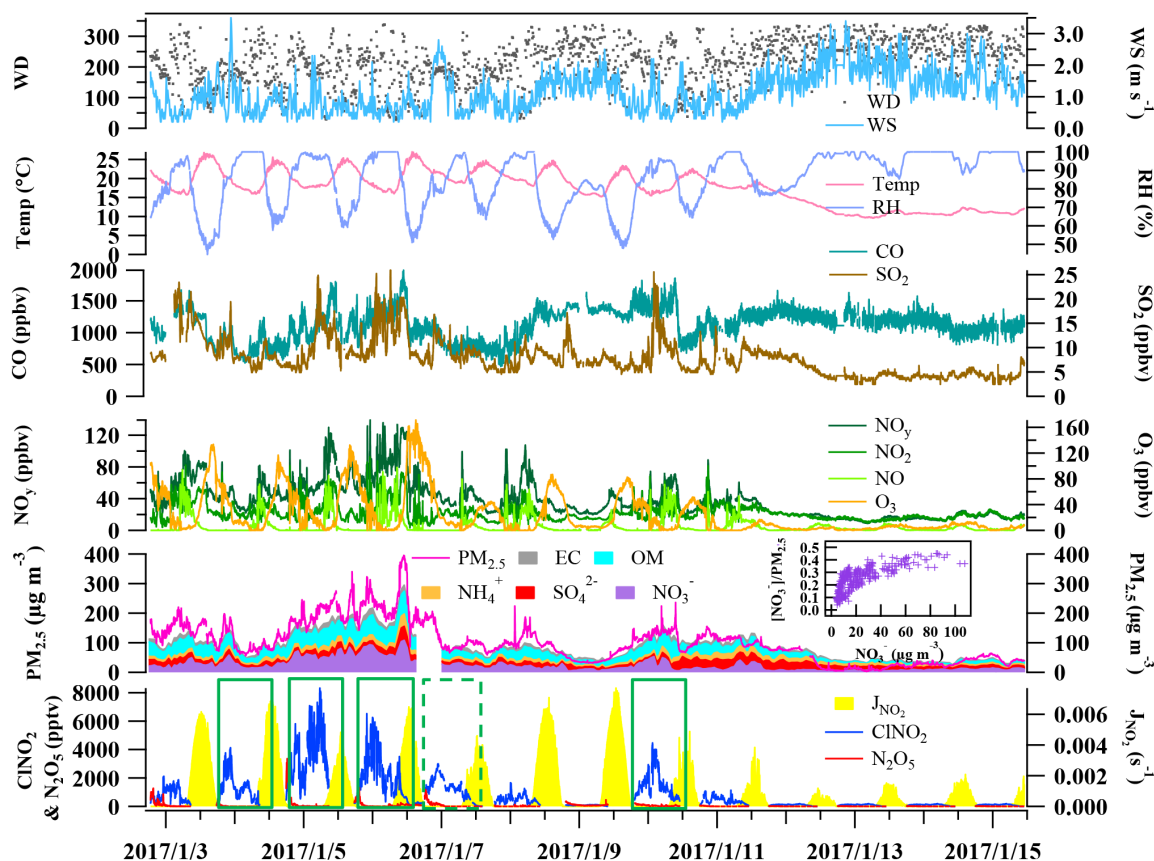
**Figure 2.** Time series of N_2O_5, $ClNO_2$, components of $PM_{2.5}$, and related trace gases and meteorological parameters from 18:40 on 2 January to 11:00 on 15 January 2017. The inset figure shows the variation of the ratio of nitrate to $PM_{2.5}$ with an increasing nitrate concentration. The green rectangles in the figure indicate the five days used for detailed analysis.
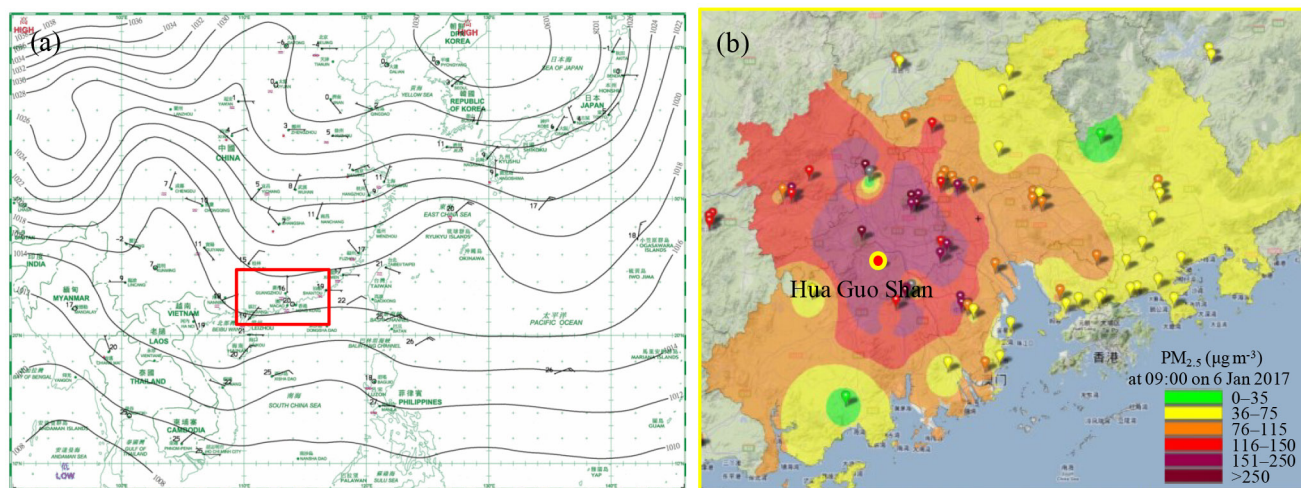
Figure 3. (a) Surface weather chart at 08:00 LT on 6 January 2017, downloaded from the Hong Kong Observatory website, indicating stagnant conditions. **(b)** The distribution of $PM_{2.5}$ concentrations in the PRD region at 09:00 LT on 6 January 2017. This figure was captured from the following website: http://113.108.142.147:20031/GDPublish/publish.aspx (last access: 17 November 2018).
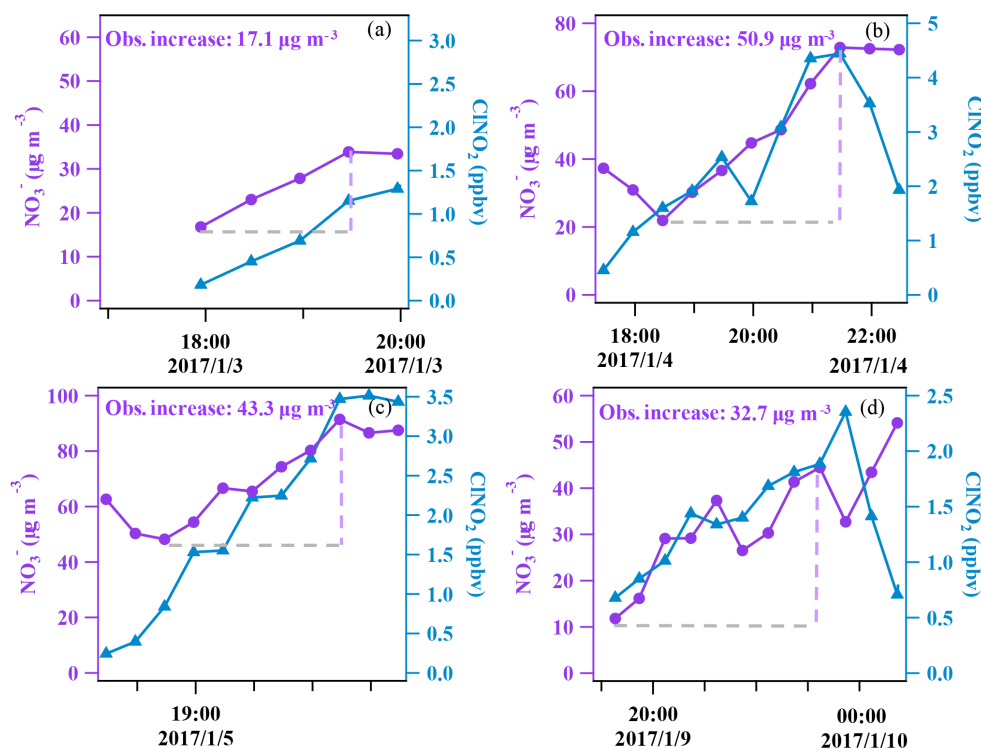
Figure 4. The covariance of aerosol nitrate and $ClNO_2$ in the early nighttime (at a 30 min time resolution) for four nights.

ably leading to the local production of $ClNO_2$ and nitrate, which was not revealed in the observed variations of $ClNO_2$ and nitrate. The concentrations of $ClNO_2$ and nitrate during this period fluctuated due to the change in the air masses indicated by the change in SO_2 concentrations and wind speeds.

3.2.2 The N_2O_5 uptake coefficient and $ClNO_2$ yield

The N_2O_5 uptake coefficient and $ClNO_2$ yield, in combination with the reactivity of NO_3 with NO and VOCs, determines the loss pathways of NO_3 and N_2O_5. To derive the uptake coefficient of N_2O_5, a method suggested by McLaren et al. (2010) was applied which treated NO_3 and N_2O_5 as a whole ($[NO_3]+[N_2O_5]$) without assuming that the chemical system was in a steady state. This approach considers that the change of NO_3 and N_2O_5 concentrations is mainly due to NO_3 / N_2O_5 chemistry; thus, it requires that the air mass has relatively stable chemical conditions and is not subject to fresh NO emissions. It also requires that $ClNO_2$ is produced from the N_2O_5 chemistry and has an increasing trend to derive the yield of $ClNO_2$. This method is applicable for the early nighttime (Fig. 5, red rectangle; Sect. 3.2.1) for these five nights.

The variation rate of $[NO_3]+[N_2O_5]$ can be calculated by deducting the production rate of $[NO_3]+[N_2O_5]$ with its loss rate as follows:

$$\frac{d([N_2O_5]+[NO_3])}{dt} = P_{NO_3} - L_{N_2O_5+NO_3} \tag{1}$$

The loss of $[NO_3]+[N_2O_5]$ is via the reaction of NO_3 with VOCs and N_2O_5 heterogeneous reactions, which can both be expressed as pseudo-first-order losses:

$$\begin{aligned} L_{N_2O_5+NO_3} &= L_{NO_3} + L_{N_2O_5} \\ &= k'_{NO_3} [NO_3] + k'_{N_2O_5} [N_2O_5], \end{aligned} \tag{2}$$

where k'_{NO_3} and $k'_{N_2O_5}$ represent the total first-order rate constants for NO_3 and N_2O_5, respectively. The loss rate of N_2O_5 can then be obtained from Eq. (3):

$$\begin{aligned} L_{N_2O_5} = k'_{N_2O_5} [N_2O_5] &= k_{NO_2+O_3} [NO_2][O_3] \\ &- \frac{d[N_2O_5]}{dt} - \frac{d[NO_3]}{dt} - k'_{NO_3} [NO_3] \end{aligned} \tag{3}$$

Because NO_3 was not measured, it was calculated by assuming an equilibrium of NO_2–NO_3–N_2O_5 as shown in Eq. (4). High levels of NO would break this equilibrium. Thus, the periods with detected NO were excluded.

Table 2. Average N_2O_5 concentration values, N_2O_5 uptake coefficients, $ClNO_2$ yields, and other related parameters and maximum $ClNO_2$ concentration values in the early nighttime for the five selected nights.

Date/time	N_2O_5 (pptv)	Max $ClNO_2$ (pptv)	NO_2 (ppbv)	O_3 (ppbv)	RH (%)	S_a ($\mu m^2\,cm^{-3}$)	P_{NO_3} (ppbv h^{-1})	k'_{NO_3} (10^{-3} s^{-1})	$L_{N_2O_5}$ (ppbv h^{-1})	$k'_{NO_3}/(K_{eq}[NO_2])$ (10^{-5} s^{-1})	$k'_{N_2O_5}$ (10^{-3} s^{-1})	$\gamma_{N_2O_5}$	ϕ_{ClNO_2}
3 January 17:40–19:00	200	1029	20	78	59	2170	4.3	0.516	4.3	3.03	8.81	0.066	0.18
4 January 17:00–22:00	700	4608	24	61	82	6452	3.3	1.54	3.2	6.07	4.16	0.009	0.32
5 January 17:00–22:00	338	4828	18	73	81	8399	3.4	0.790	3.3	4.06	9.00	0.015	0.29
6 January 17:00–22:40	326	2908	13	82	77	5092	2.8	0.677	2.6	4.95	3.78	0.013	0.20
9 January 19:00–00:20	121	2553	19	41	85	5173	1.9	0.516	1.9	1.40	4.28	0.015	0.28
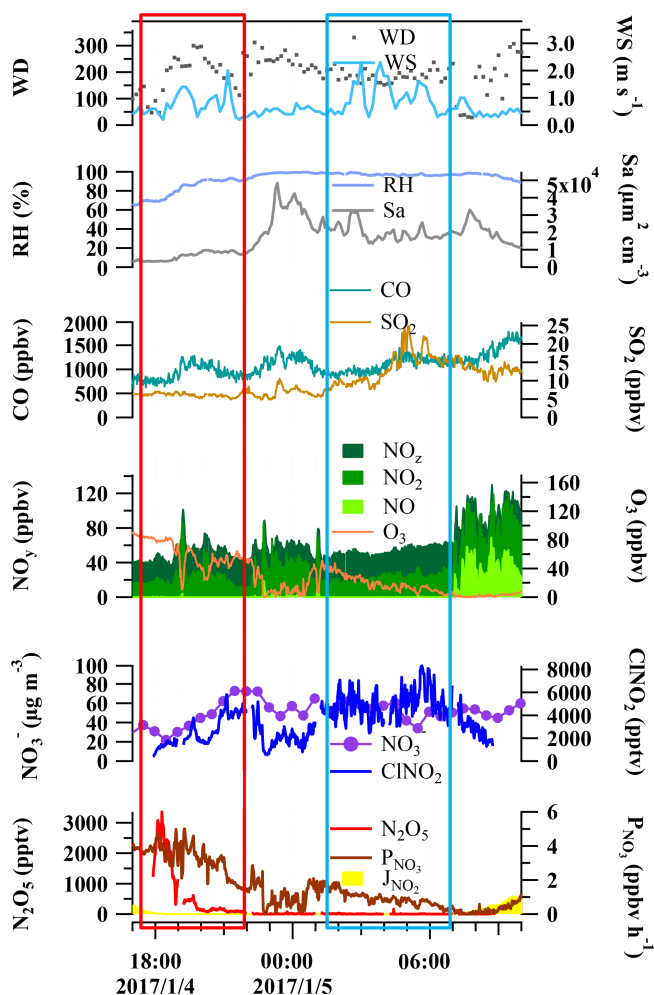
Figure 5. Variation of N_2O_5, $ClNO_2$, NO_3^-, and trace gases and meteorological conditions during the night from 4 to 5 January 2017 as an example from the five selected nights.

$d[NO_3]/dt$ and $d[N_2O_5]/dt$ were calculated as the rate of change of NO_3 and N_2O_5, respectively, at a time resolution of 10 min. k'_{NO_3} was derived using the measured concentrations of NMHCs as in Eq. (5) by interpolating the data of the NMHCs to a 10 min time resolution. The NO_3 reactivity with VOCs (k'_{NO_3}) in the early nighttime ranged from 0.516 to 1.54×10^{-3} s^{-1} (Table 2), which was higher than those derived at Mt. TMS in winter 2013 (0.17 to 1.1×10^{-3} s^{-1})

(Brown et al., 2016), but lower than those in the North China Plain during the summertime (2 to 57×10^{-3} s^{-1}) (Tham et al., 2016; H. Wang et al., 2017, 2018b; Z. Wang et al., 2017). NMHCs were not measured from 9 to 10 January 2017. We used the average k'_{NO_3} in the early nighttime from 3 to 4 January as a replacement because these two periods had similar pollution levels for most pollutants. For the later nighttime (Fig. 5, blue rectangle), low levels of N_2O_5 and moderate levels of P_{NO_3} made Eq. (3) inapplicable even though NO was not detected.

$$[NO_3] = \frac{[N_2O_5]}{[NO_2]\cdot K_{eq}} \quad (4)$$

$$k'_{NO_3} = \sum k_i[VOC_i] \quad (5)$$

Finally, the uptake coefficient of N_2O_5 was derived using Eq. (6) for every 10 min and averaged for each selected period. In Eq. (6), $C_{N_2O_5}$ is the mean molecular speed of N_2O_5, and S_a is the aerosol surface area density. The yield of $ClNO_2$ was derived via dividing the integrated production of $ClNO_2$ ($[ClNO_2]_{max}$) by the integrated loss of N_2O_5 since sunset as Eq. (7).

$$k'_{N_2O_5} = \frac{L_{N_2O_5}}{[N_2O_5]} = \frac{1}{4}C_{N_2O_5}S_a\gamma_{N_2O_5} \quad (6)$$

$$\phi = \frac{[ClNO_2]_{max}}{\int L_{N_2O_5}dt} \quad (7)$$

The relative importance of the NO_3 reactions with VOCs and N_2O_5 heterogeneous reactions can be examined by comparing the values of the loss coefficient of the NO_3 reactions $\left(\frac{k'_{NO_3}}{[NO_2]\cdot K_{eq}}\right)$ and N_2O_5 heterogeneous reactions ($k'_{N_2O_5}$) (Tham et al., 2016). Based on the calculations, the values of $\frac{k'_{NO_3}}{[NO_2]\cdot K_{eq}}$ were 1.40×10^{-5} to 6.07×10^{-5} s^{-1} (see Table 2), while those of $k'_{N_2O_5}$ were 3.78×10^{-3} to 9.00×10^{-3} s^{-1}, which was 2 orders of magnitude higher than $\frac{k'_{NO_3}}{[NO_2]\cdot K_{eq}}$, suggesting that N_2O_5 heterogeneous reactions were the dominant loss pathway for both NO_3 and N_2O_5.

The average $\gamma_{N_2O_5}$ and ϕ_{ClNO_2} derived for the early night in the five cases are listed in Table 2. The data show that the uptake coefficient ranged from 0.009 to 0.066, which was comparable with previous values derived at Mt. Tai Mo Shan (TMS) in Hong Kong (0.004 to 0.022) (Brown et al., 2016)

Table 3. Average values of the N_2O_5 loss rate and related parameters for selected periods in the later nighttime.

Date/time	NO_2 (ppbv)	O_3 (ppbv)	P_{NO_3} (ppbv h^{-1})	k'_{NO_3} (10^{-3} s^{-1})	$L_{N_2O_5}$ (ppbv h^{-1})
3–4 January 21:00–05:00	20.8	20.7	1.00	0.684	1.00
5 January 01:30–06:50	22.4	19.5	0.96	1.45	0.96
5–6 January 23:40–01:10	21.1	25.5	1.26	1.13	1.26
6–7 January 23:00–06:00	22.1	14.4	0.82	0.709	0.82
10 January 01:50–03:30	24.8	15.6	0.90	–	0.90

and in the North China Plain (0.006 to 0.102) (Tham et al., 2016, 2018; H. Wang et al., 2017, 2018b; X. Wang et al., 2017; Z. Wang et al., 2017; Zhou et al., 2018). It is interesting to see a much higher $\gamma_{N_2O_5}$ value (0.066) on 3 January than those on other four nights (0.009–0.015), which resulted from higher P_{NO_3} but much lower Sa and relatively low N_2O_5 concentrations on 3 January. We examined known factors affecting the loss of NO_3 and N_2O_5 such as the concentrations of NO, NMHCs, and aerosol compositions, but found no obvious difference between 3 January and the other nights. The yield in this study varied from 0.18 to 0.32, which was similar to most studies in China (Tham et al., 2016, 2018; Z. Wang et al., 2017; Yun et al., 2018; Zhou et al., 2018).

The uncertainty of the above $\gamma_{N_2O_5}$ was estimated to be $\pm 45\%$ due to the measurement uncertainty of N_2O_5 ($\pm 25\%$), NO_2 ($\pm 20\%$), O_3 ($\pm 5\%$), and Sa ($\pm 30\%$). The uncertainty of ϕ_{ClNO_2} was mainly caused by the uncertainty of NO_2 ($\pm 20\%$), O_3 ($\pm 5\%$), and $ClNO_2$ ($\pm 25\%$) and was estimated to be $\pm 30\%$. The correlation between $\gamma_{N_2O_5}$, ϕ_{ClNO_2}, and the concentrations of aerosol compositions (see Table S2) or RH was investigated, and the results (not shown here) did not indicate any significant dependence of $\gamma_{N_2O_5}$ or ϕ_{ClNO_2} on these parameters.

3.3 Nitrate formation potential $p(NO_3^-)$ through N_2O_5 chemistry

3.3.1 Nighttime $p(NO_3^-)$

The formation potential of NO_3^- through N_2O_5 chemistry is the total amount of NO_3^- accumulated from N_2O_5 heterogeneous loss. It can be calculated by deducting the integrated production of $ClNO_2$ from the integrated loss of N_2O_5 as follows:

$$p(NO_3^-) = (2 - \phi) \int L_{N_2O_5} \mathrm{d}t$$
$$= 2 \int L_{N_2O_5} \mathrm{d}t - [ClNO_2]_{max} \quad (8)$$

In the early nighttime, the average loss rate of N_2O_5 ($L_{N_2O_5}$) ranged from 1.9 to 4.3 ppbv h^{-1} (Table 2), which was close to the average P_{NO_3} due to the dominance of the N_2O_5 heterogeneous reactions in NO_3 and N_2O_5 loss. Based
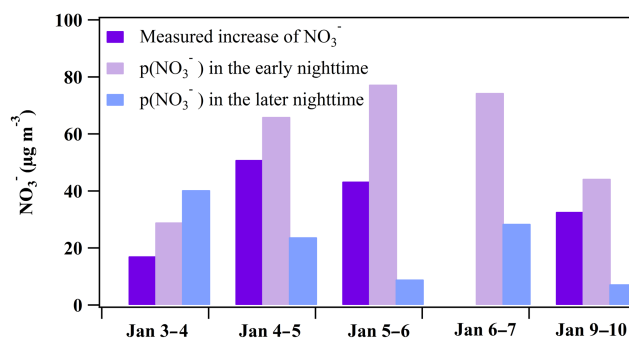
Figure 6. Comparison between the measured NO_3^- increase and the NO_3^- formation potential in the early nighttime (periods in Table 2: 3 January 17:40–19:00, 4 January 17:00–22:00, 5 January 17:00–22:00, 6 January 17:00–22:40, and 9 January 19:00–00:20) and in the later nighttime (periods in Table 3: 3–4 January 21:00–05:00, 5 January 01:30–06:50, 5–6 January 23:40–01:10, 6–7 January 23:00–06:00, and 10 January 01:50–03:30).

on the derived N_2O_5 loss rate and the maximum $ClNO_2$ concentration, the formation potential of NO_3^- was derived and ranged from 29.0 to 77.3 µg m^{-3} as shown in Fig. 6. The measured increase of the NO_3^- concentration in the early nighttime can be completely explained by the integrated production of NO_3^- via the N_2O_5 heterogeneous reactions during the same period.

In the later nighttime, the method described in Sect. 3.2.2 was not valid for calculating the N_2O_5 heterogeneous loss rate as mentioned above. We attempted to estimate the formation potential of nitrate by assuming that the N_2O_5 heterogeneous reactions continued to dominate the loss of NO_3 + N_2O_5 in the later nighttime. The k'_{NO_3} values in the later nighttime were comparable to those in the early nighttime, and the high RH (close to 100 %) in the later nighttime was favorable for N_2O_5 heterogeneous reactions. We assumed that all NO_3 was quickly consumed by the N_2O_5 heterogeneous reactions, which means that the loss rate of N_2O_5 approximated to the production rate of NO_3 ($L_{N_2O_5} \approx P_{NO_3}$). As listed in Table 3, the N_2O_5 loss rates ranged from 0.82 to 1.26 ppbv h^{-1}, which were significantly lower than those derived in the early nighttime. The derived N_2O_5 loss rate here and the yield of $ClNO_2$ in the early nighttime were used to es-
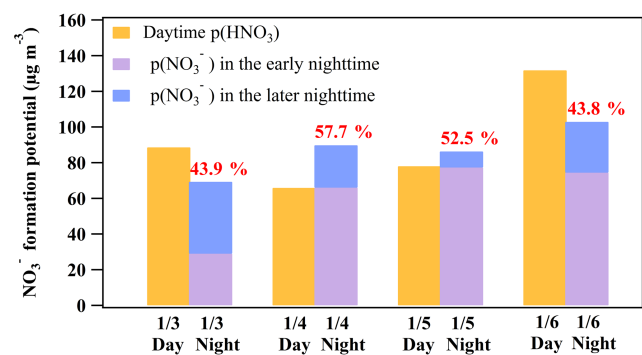
Figure 7. Comparison between the daytime (07:00 to 17:00 LT; assuming that all gas-phase HNO_3 is partitioned into particle phase) and nighttime (17:00 to 07:00 LT of the next day) NO_3^- formation potential. The early nighttime of each day represents the periods in Table 2, including 3 January 17:40–19:00, 4 January 17:00–22:00, 5 January 17:00–22:00, 6 January 17:00–22:40, and 9 January 19:00–00:20. The later nighttime of each day represents the periods in Table 3, including 3–4 January 21:00–05:00, 5 January 01:30–06:50, 5–6 January 23:40–01:10, 6–7 January 23:00–06:00, and 10 January 01:50–03:30. The intercomparison of the NO_3^- formation potential during the day and night on 9 and 10 January was not conducted due to the lack of NMHC data after 8 January which made the model simulation of OH infeasible during the day on 9 January.

timate the formation potential of NO_3^- in the later nighttime. As shown in Fig. 6, the nitrate produced during these later periods ranged from 7.3 to 40.3 µg m^{-3}, which was lower than values in the early nighttime for four nights, indicating that the nighttime nitrate from N_2O_5 chemistry was mainly produced in the early nighttime.

3.3.2 Comparison with the daytime production of HNO_3

During the daytime, the formation of NO_3^- is mainly from the gas–particle partitioning of the gas-phase HNO_3 formed via the $OH + NO_2$ reaction. Hence, the daytime formation potential of HNO_3 ($p(HNO_3)$) can be treated as the upper limit for the locally produced daytime aerosol nitrate. To calculate the daytime $p(HNO_3)$, a box model based on MCM v3.3.1 was used to derive the mixing ratio of OH and the rates of $OH + NO_2$ as described in Sect. 2.4. This model was previously used in our study at Wangdu in northern China (Tham et al., 2016). The calculated mixing ratios of OH at Wangdu with this model compared well with those observed by the laser-induced fluorescence (LIF) technique (Tan et al., 2017). In the present study, the average daytime OH (07:00 to 17:00) mixing ratios were 1.71 to 3.82 × 10^6 molec cm^{-3} from 3 to 7 January, as listed in Table 4, with the maximum values reaching 3.24 to 6.71 × 10^6 molec cm^{-3}. The detailed results for OH can be found in Fig. S3.

Table 4. Average OH mixing ratio and rate of $OH + NO_2$ during the daytime (07:00 to 17:00 LT) from 3 to 7 January 2017.

Date	OH (molec cm^{-3})	NO_2 (ppbv)	$OH + NO_2$ (ppbv h^{-1})
3 January	2.18×10^6	36.2	3.49
4 January	2.47×10^6	23.6	2.60
5 January	2.62×10^6	30.8	3.09
6 January	3.82×10^6	31.5	5.21
7 January	1.71×10^6	18.4	1.40

The average production rates of HNO_3 via the $OH + NO_2$ reaction were 1.40 to 5.21 ppbv h^{-1} from 3 to 7 January, and the integrated formation potential of HNO_3 during the daytime was 35.7 to 131.8 µg m^{-3}, which was comparable to the nighttime $p(NO_3^-)$ that ranged from 69.3 to 102.9 µg m^{-3} (Fig. 7). The nighttime production of nitrate via the heterogeneous uptake of N_2O_5 accounted for 43.8 % to 57.7 % of the total nitrate ($NO_3^- + HNO_3$) produced in a 24 h period at the site. These results underscored the important role of N_2O_5 heterogeneous chemistry in nitrate formation in this severe winter haze in southern China.

4 Concluding remarks

With the use of concurrent measurements of nitrate, $ClNO_2$, and related pollutants, this study demonstrates the important contribution of N_2O_5 heterogeneous uptake in nitrate formation. Current chemical transport models have difficulties simulating this nitrate production pathway. Therefore, more research efforts are needed to improve the representations of $\gamma_{N_2O_5}$ and ϕ_{ClNO_2} for the better prediction of nitrate in the models. The observation-based approach presented here can be applied to investigate nitrate formation in other areas.

Author contributions. TW designed the research. WW conducted the CIMS measurements, and YZ, DY, HY, MX, CY, and PS performed the measurements of the other parameters used in this study. HY, TW, MX, and WW analyzed the data. HY and TW wrote the paper, and all authors contributed to discussion and commented on the paper.

References

Anttila, T., Kiendler-Scharr, A., Tillmann, R., and Mentel, T. F.: On the reactive uptake of gaseous compounds by organic-coated aqueous aerosols: Theoretical analysis and application to the heterogeneous hydrolysis of N_2O_5, J. Phys. Chem. A, 110, 10435–10443, 2006.

Bauer, J. J., Yu, X.-Y., Cary, R., Laulainen, N., and Berkowitz, C.: Characterization of the sunset semi-continuous carbon aerosol analyzer, J. Air Waste Manage., 59, 826–833, 2009.

Bertram, T. H. and Thornton, J. A.: Toward a general parameterization of N_2O_5 reactivity on aqueous particles: the competing effects of particle liquid water, nitrate and chloride, Atmos. Chem. Phys., 9, 8351–8363, https://doi.org/10.5194/acp-9-8351-2009, 2009.

Brown, S. S. and Stutz, J.: Nighttime radical observations and chemistry, Chem. Soc. Rev., 41, 6405–6447, 2012.

Brown, S. S., Dubé, W. P., Tham, Y. J., Zha, Q., Xue, L., Poon, S., Wang, Z., Blake, D. R., Tsui, W., and Parrish, D. D.: Nighttime Chemistry at a High Altitude Site Above Hong Kong, J. Geophys. Res.-Atmos., 121, 2457–2475, https://doi.org/10.1002/2015JD024566, 2016.

Chang, W. L., Bhave, P. V., Brown, S. S., Riemer, N., Stutz, J., and Dabdub, D.: Heterogeneous Atmospheric Chemistry, Ambient Measurements, and Model Calculations of N_2O_5: A Review, Aerosol Sci. Tech., 45, 665–695, https://doi.org/10.1080/02786826.2010.551672, 2011.

Cui, L., Zhang, Z., Huang, Y., Lee, S. C., Blake, D. R., Ho, K. F., Wang, B., Gao, Y., Wang, X. M., and Louie, P. K. K.: Measuring OVOCs and VOCs by PTR-MS in an urban roadside microenvironment of Hong Kong: relative humidity and temperature dependence, and field intercomparisons, Atmos. Meas. Tech., 9, 5763–5779, https://doi.org/10.5194/amt-9-5763-2016, 2016.

Davis, J. M., Bhave, P. V., and Foley, K. M.: Parameterization of N2O5 reaction probabilities on the surface of particles containing ammonium, sulfate, and nitrate, Atmos. Chem. Phys., 8, 5295–5311, https://doi.org/10.5194/acp-8-5295-2008, 2008.

Dentener, F. J. and Crutzen, P. J.: Reaction of N_2O_5 on tropospheric aerosols: Impact on the global distributions of NO_x, O_3, and OH, J. Geophys. Res.-Atmos., 98, 7149–7163, 1993.

Dong, H.-B., Zeng, L.-M., Hu, M., Wu, Y.-S., Zhang, Y.-H., Slanina, J., Zheng, M., Wang, Z.-F., and Jansen, R.: Technical Note: The application of an improved gas and aerosol collector for ambient air pollutants in China, Atmos. Chem. Phys., 12, 10519–10533, https://doi.org/10.5194/acp-12-10519-2012, 2012.

Evans, M. J. and Jacob, D. J.: Impact of new laboratory studies of N_2O_5 hydrolysis on global model budgets of tropospheric nitrogen oxides, ozone, and OH, Geophys. Res. Lett., 32, L09813, https://doi.org/10.1029/2005GL022469, 2005.

Finlayson-Pitts, B. J., Ezell, M. J., and Pitts, J. N.: Formation of chemically active chlorine compounds by reactions of atmospheric NaCl particles with gaseous N_2O_5 and $ClONO_2$, Nature, 337, 241–244, 1989.

Fu, X., Wang, X., Guo, H., Cheung, K., Ding, X., Zhao, X., He, Q., Gao, B., Zhang, Z., and Liu, T.: Trends of ambient fine particles and major chemical components in the Pearl River Delta region: observation at a regional background site in fall and winter, Sci. Total Environ., 497, 274–281, 2014.

Ge, X., He, Y., Sun, Y., Xu, J., Wang, J., Shen, Y., and Chen, M.: Characteristics and formation mechanisms of fine particulate nitrate in typical urban areas in China, Atmosphere, 8, 62, https://doi.org/10.3390/atmos8030062, 2017.

Geng, G., Zhang, Q., Tong, D., Li, M., Zheng, Y., Wang, S., and He, K.: Chemical composition of ambient $PM_{2.5}$ over China and relationship to precursor emissions during 2005–2012, Atmos. Chem. Phys., 17, 9187–9203, https://doi.org/10.5194/acp-17-9187-2017, 2017.

Hennig, T., Massling, A., Brechtel, F., and Wiedensohler, A.: A tandem DMA for highly temperature-stabilized hygroscopic particle growth measurements between 90 % and 98 % relative humidity, J. Aerosol Sci., 36, 1210–1223, 2005.

Huang, R. J., Zhang, Y. L., Bozzetti, C., Ho, K. F., Cao, J. J., Han, Y. M., Daellenbach, K. R., Slowik, J. G., Platt, S. M., Canonaco, F., Zotter, P., Wolf, R., Pieber, S. M., Bruns, E. A., Crippa, M., Ciarelli, G., Piazzalunga, A., Schwikowski, M., Abbaszade, G., Schnelle-Kreis, J., Zimmermann, R., An, Z. S., Szidat, S., Baltensperger, U., El Haddad, I., and Prevot, A. S. H.: High secondary aerosol contribution to particulate pollution during haze events in China, Nature, 514, 218–222, https://doi.org/10.1038/Nature13774, 2014.

Jenkin, M. E., Saunders, S. M., Wagner, V., and Pilling, M. J.: Protocol for the development of the Master Chemical Mechanism, MCM v3 (Part B): tropospheric degradation of aromatic volatile organic compounds, Atmos. Chem. Phys., 3, 181–193, https://doi.org/10.5194/acp-3-181-2003, 2003.

Jenkin, M. E., Young, J. C., and Rickard, A. R.: The MCM v3.3.1 degradation scheme for isoprene, Atmos. Chem. Phys., 15, 11433–11459, https://doi.org/10.5194/acp-15-11433-2015, 2015.

Li, H., Zhang, Q., Zheng, B., Chen, C., Wu, N., Guo, H., Zhang, Y., Zheng, Y., Li, X., and He, K.: Nitrate-driven urban haze pollution during summertime over the North China Plain, Atmos. Chem. Phys., 18, 5293–5306, https://doi.org/10.5194/acp-18-5293-2018, 2018.

Liu, H. J., Zhao, C. S., Nekat, B., Ma, N., Wiedensohler, A., van Pinxteren, D., Spindler, G., Müller, K., and Herrmann, H.: Aerosol hygroscopicity derived from size-segregated chemical composition and its parameterization in the North China Plain, Atmos. Chem. Phys., 14, 2525–2539, https://doi.org/10.5194/acp-14-2525-2014, 2014.

Li, W., Liu, X., Zhang, Y., Sun, K., Wu, Y., Xue, R., Zeng, L., Qu, Y., and An, J.: Characteristics and formation mechanism of regional haze episodes in the Pearl River Delta of China, J. Environ. Sci., 63, 236–249, 2017.

Liu, X., Sun, K., Qu, Y., Hu, M., Sun, Y., Zhang, F., and Zhang, Y.: Secondary formation of sulfate and nitrate during a haze episode in megacity Beijing, China, Aerosol Air Qual. Res., 15, 2246–2257, 2015.

Makar, P., Wiebe, H., Staebler, R., Li, S., and Anlauf, K.: Measurement and modeling of particle nitrate formation, J. Geophys. Res.-Atmos., 103, 13095–13110, 1998.

McDuffie, E. E., Fibiger, D. L., Dubé, W. P., Lopez-Hilfiker, F., Lee, B. H., Thornton, J. A., Shah, V., Jaeglé, L., Guo, H., and Weber, R. J.: Heterogeneous N_2O_5 uptake during winter: Aircraft measurements during the 2015 WINTER campaign and critical evaluation of current parameterizations, J. Geophys. Res.-Atmos., 123, 4345–4372, https://doi.org/10.1002/2018JD028336, 2018.

McLaren, R., Wojtal, P., Majonis, D., McCourt, J., Halla, J. D., and Brook, J.: NO_3 radical measurements in a polluted marine environment: links to ozone formation, Atmos. Chem. Phys., 10, 4187–4206, https://doi.org/10.5194/acp-10-4187-2010, 2010.

Munger, J. W., Fan, S. M., Bakwin, P. S., Goulden, M. L., Goldstein, A., Colman, A. S., and Wofsy, S. C.: Regional budgets for nitrogen oxides from continental sources: Variations of rates for oxidation and deposition with season and distance from source regions, J. Geophys. Res.-Atmos., 103, 8355–8368, 1998.

Pathak, R. K., Wu, W. S., and Wang, T.: Summertime $PM_{2.5}$ ionic species in four major cities of China: nitrate formation in an ammonia-deficient atmosphere, Atmos. Chem. Phys., 9, 1711–1722, https://doi.org/10.5194/acp-9-1711-2009, 2009.

Pathak, R. K., Wang, T., and Wu, W. S.: Nighttime enhancement of $PM_{2.5}$ nitrate in ammonia-poor atmospheric conditions in Beijing and Shanghai: Plausible contributions of heterogeneous hydrolysis of N_2O_5 and HNO_3 partitioning, Atmos. Environ., 45, 1183–1191, https://doi.org/10.1016/j.atmosenv.2010.09.003, 2011.

Phillips, G. J., Thieser, J., Tang, M., Sobanski, N., Schuster, G., Fachinger, J., Drewnick, F., Borrmann, S., Bingemer, H., Lelieveld, J., and Crowley, J. N.: Estimating N_2O_5 uptake coefficients using ambient measurements of NO_3, N_2O_5, $ClNO_2$ and particle-phase nitrate, Atmos. Chem. Phys., 16, 13231–13249, https://doi.org/10.5194/acp-16-13231-2016, 2016.

Qu, Z., Henze, D. K., Capps, S. L., Wang, Y., Xu, X., Wang, J., and Keller, M.: Monthly top-down NO_x emissions for China (2005–2012): A hybrid inversion method and trend analysis, J. Geophys. Res.-Atmos., 122, 4600–4625, 2017.

Reuter, M., Buchwitz, M., Hilboll, A., Richter, A., Schneising, O., Hilker, M., Heymann, J., Bovensmann, H., and Burrows, J.: Decreasing emissions of NO_x relative to CO_2 in East Asia inferred from satellite observations, Nat. Geosci., 7, 792–795, https://doi.org/10.1038/NGEO2257, 2014.

Riemer, N., Vogel, H., Vogel, B., Schell, B., Ackermann, I., Kessler, C., and Hass, H.: Impact of the heterogeneous hydrolysis of N_2O_5 on chemistry and nitrate aerosol formation in the lower troposphere under photosmog conditions, J. Geophys. Res., 108, 4144, https://doi.org/10.1029/2002JD002436, 2003.

Riemer, N., Vogel, H., Vogel, B., Anttila, T., Kiendler, Scharr, A., and Mentel, T.: Relative importance of organic coatings for the heterogeneous hydrolysis of N_2O_5 during summer in Europe, J. Geophys. Res., 114, D17307, https://doi.org/10.1029/2008JD011369, 2009.

Roberts, J. M., Osthoff, H. D., Brown, S. S., Ravishankara, A., Coffman, D., Quinn, P., and Bates, T.: Laboratory studies of products of N_2O_5 uptake on Cl-containing substrates, Geophys. Res. Lett., 36, L20808, https://doi.org/10.1029/2009GL040448, 2009.

Saunders, S. M., Jenkin, M. E., Derwent, R. G., and Pilling, M. J.: Protocol for the development of the Master Chemical Mechanism, MCM v3 (Part A): tropospheric degradation of non-aromatic volatile organic compounds, Atmos. Chem. Phys., 3, 161–180, https://doi.org/10.5194/acp-3-161-2003, 2003.

Schaap, M., van Loon, M., ten Brink, H. M., Dentener, F. J., and Builtjes, P. J. H.: Secondary inorganic aerosol simulations for Europe with special attention to nitrate, Atmos. Chem. Phys., 4, 857–874, https://doi.org/10.5194/acp-4-857-2004, 2004.

Seinfeld, J. H. and Pandis, S. N.: Atmospheric chemistry and physics: from air pollution to climate change, John Wiley & Sons, New York, 2016.

Sun, Y., Chen, C., Zhang, Y., Xu, W., Zhou, L., Cheng, X., Zheng, H., Ji, D., Li, J., and Tang, X.: Rapid formation and evolution of an extreme haze episode in Northern China during winter 2015, Sci. Rep., 6, 27151, https://doi.org/10.1038/srep27151, 2016.

Tan, Z., Fuchs, H., Lu, K., Hofzumahaus, A., Bohn, B., Broch, S., Dong, H., Gomm, S., Häseler, R., He, L., Holland, F., Li, X., Liu, Y., Lu, S., Rohrer, F., Shao, M., Wang, B., Wang, M., Wu, Y., Zeng, L., Zhang, Y., Wahner, A., and Zhang, Y.: Radical chemistry at a rural site (Wangdu) in the North China Plain: observation and model calculations of OH, HO_2 and RO_2 radicals, Atmos. Chem. Phys., 17, 663–690, https://doi.org/10.5194/acp-17-663-2017, 2017.

Tham, Y. J., Wang, Z., Li, Q., Yun, H., Wang, W., Wang, X., Xue, L., Lu, K., Ma, N., Bohn, B., Li, X., Kecorius, S., Größ, J., Shao, M., Wiedensohler, A., Zhang, Y., and Wang, T.: Significant concentrations of nitryl chloride sustained in the morning: investigations of the causes and impacts on ozone production in a polluted region of northern China, Atmos. Chem. Phys., 16, 14959–14977, https://doi.org/10.5194/acp-16-14959-2016, 2016.

Tham, Y. J., Wang, Z., Li, Q., Wang, W., Wang, X., Lu, K., Ma, N., Yan, C., Kecorius, S., Wiedensohler, A., Zhang, Y., and Wang, T.: Heterogeneous N_2O_5 uptake coefficient and production yield of $ClNO_2$ in polluted northern China: roles of aerosol water content and chemical composition, Atmos. Chem. Phys., 18, 13155–13171, https://doi.org/10.5194/acp-18-13155-2018, 2018.

Trebs, I., Bohn, B., Ammann, C., Rummel, U., Blumthaler, M., Königstedt, R., Meixner, F. X., Fan, S., and Andreae, M. O.: Relationship between the NO_2 photolysis frequency and the solar global irradiance, Atmos. Meas. Tech., 2, 725–739, https://doi.org/10.5194/amt-2-725-2009, 2009.

Wang, H., Lu, K., Chen, X., Zhu, Q., Chen, Q., Guo, S., Jiang, M., Li, X., Shang, D., Tan, Z., Wu, Y., Wu, Z., Zou, Q., Zheng, Y., Zeng, L., Zhu, T., Hu, M., and Zhang, Y.: High N_2O_5 Concentrations Observed in Urban Beijing: Implications of a Large Ni-

trate Formation Pathway, Environ. Sci. Tech. Lett., 4, 416–420, https://doi.org/10.1021/acs.estlett.7b00341, 2017.

Wang, H., Lu, K., Chen, X., Zhu, Q., Wu, Z., Wu, Y., and Sun, K.: Fast particulate nitrate formation via N_2O_5 uptake aloft in winter in Beijing, Atmos. Chem. Phys., 18, 10483–10495, https://doi.org/10.5194/acp-18-10483-2018, 2018a.

Wang, H., Lu, K., Guo, S., Wu, Z., Shang, D., Tan, Z., Wang, Y., Le Breton, M., Lou, S., Tang, M., Wu, Y., Zhu, W., Zheng, J., Zeng, L., Hallquist, M., Hu, M., and Zhang, Y.: Efficient N_2O_5 uptake and NO_3 oxidation in the outflow of urban Beijing, Atmos. Chem. Phys., 18, 9705–9721, https://doi.org/10.5194/acp-18-9705-2018, 2018b.

Wang, M., Zeng, L., Lu, S., Shao, M., Liu, X., Yu, X., Chen, W., Yuan, B., Zhang, Q., Hu, M., and Zhang, Z.: Development and validation of a cryogen-free automatic gas chromatograph system (GC-MS/FID) for online measurements of volatile organic compounds, Anal. Methods, 6, 9424–9434, https://doi.org/10.1039/C4AY01855A, 2014.

Wang, T., Tham, Y. J., Xue, L., Li, Q., Zha, Q., Wang, Z., Poon, S. C., Dubé, W. P., Blake, D. R., and Louie, P. K.: Observations of nitryl chloride and modeling its source and effect on ozone in the planetary boundary layer of southern China, J. Geophys. Res.-Atmos., 121, 2476–2489, https://doi.org/10.1002/2015JD024556, 2016.

Wang, X., Zhang, Y., Chen, H., Yang, X., Chen, J., and Geng, F.: Particulate nitrate formation in a highly polluted urban area: a case study by single-particle mass spectrometry in Shanghai, Environ. Sci. Technol., 43, 3061–3066, 2009.

Wang, X., Chen, W., Chen, D., Wu, Z., and Fan, Q.: Long-term trends of fine particulate matter and chemical composition in the Pearl River Delta Economic Zone (PRDEZ), China, Front. Environ. Sci. Eng., 10, 53–62, 2016.

Wang, X., Wang, H., Xue, L., Wang, T., Wang, L., Gu, R., Wang, W., Tham, Y. J., Wang, Z., Yang, L., Chen, J., and Wang, W.: Observations of N_2O_5 and $ClNO_2$ at a polluted urban surface site in North China: High N_2O_5 uptake coefficients and low $ClNO_2$ product yields, Atmos. Environ., 156, 125–134, 2017.

Wang, Z., Wang, W., Tham, Y. J., Li, Q., Wang, H., Wen, L., Wang, X., and Wang, T.: Fast heterogeneous N_2O_5 uptake and ClNO2 production in power plant and industrial plumes observed in the nocturnal residual layer over the North China Plain, Atmos. Chem. Phys., 17, 12361–12378, https://doi.org/10.5194/acp-17-12361-2017, 2017.

Wen, L., Chen, J., Yang, L., Wang, X., Xu, C., Sui, X., Yao, L., Zhu, Y., Zhang, J., and Zhu, T.: Enhanced formation of fine particulate nitrate at a rural site on the North China Plain in summer: The important roles of ammonia and ozone, Atmos. Environ., 101, 294–302, 2015.

Wen, L., Xue, L., Wang, X., Xu, C., Chen, T., Yang, L., Wang, T., Zhang, Q., and Wang, W.: Summertime fine particulate nitrate pollution in the North China Plain: increasing trends, formation mechanisms and implications for control policy, Atmos. Chem. Phys., 18, 11261–11275, https://doi.org/10.5194/acp-18-11261-2018, 2018.

Xu, Z., Wang, T., Xue, L. K., Louie, P. K. K., Luk, C. W. Y., Gao, J., Wang, S. L., Chai, F. H., and Wang, W. X.: Evaluating the uncertainties of thermal catalytic conversion in measuring atmospheric nitrogen dioxide at four differently polluted sites in China, Atmos. Environ., 76, 221–226, 2013.

Xu, Z., Wang, T., Wu, J., Xue, L., Chan, J., Zha, Q., Zhou, S., Louie, P. K. K., and Luk, C. W. Y.: Nitrous acid (HONO) in a polluted subtropical atmosphere: Seasonal variability, direct vehicle emissions and heterogeneous production at ground surface, Atmos. Environ., 106, 100–109, 2015.

Xue, J., Yuan, Z., Lau, A. K., and Yu, J. Z.: Insights into factors affecting nitrate in $PM_{2.5}$ in a polluted high NO_x environment through hourly observations and size distribution measurements, J. Geophys. Res.-Atmos., 119, 4888–4902, 2014.

Xue, L. K., Saunders, S. M., Wang, T., Gao, R., Wang, X. F., Zhang, Q. Z., and Wang, W. X.: Development of a chlorine chemistry module for the Master Chemical Mechanism, Geosci. Model Dev., 8, 3151–3162, https://doi.org/10.5194/gmd-8-3151-2015, 2015.

Yang, T., Sun, Y., Zhang, W., Wang, Z., Liu, X., Fu, P., and Wang, X.: Evolutionary processes and sources of high-nitrate haze episodes over Beijing, Spring, J. Environ. Sci., 54, 142–151, 2017.

Yue, D., Zhong, L., Zhang, T., Shen, J., Zhou, Y., Zeng, L., Dong, H., and Ye, S.: Pollution properties of water-soluble secondary inorganic ions in atmospheric $PM_{2.5}$ in the Pearl River Delta region, Aerosol Air Qual. Res., 15, 1737–1747, 2015.

Yun, H., Wang, T., Wang, W., Tham, Y. J., Li, Q., Wang, Z., and Poon, S. C. N.: Nighttime NO_x loss and $ClNO_2$ formation in the residual layer of a polluted region: Insights from field measurements and an iterative box model, Sci. Total Environ., 622–623, 727–734, 2018.

Zhang, R., Wang, G., Guo, S., Zamora, M. L., Ying, Q., Lin, Y., Wang, W., Hu, M., and Wang, Y.: Formation of Urban Fine Particulate Matter, Chem. Rev., 115, 3803–3855, https://doi.org/10.1021/acs.chemrev.5b00067, 2015.

Zhou, W., Zhao, J., Ouyang, B., Mehra, A., Xu, W., Wang, Y., Bannan, T. J., Worrall, S. D., Priestley, M., Bacak, A., Chen, Q., Xie, C., Wang, Q., Wang, J., Du, W., Zhang, Y., Ge, X., Ye, P., Lee, J. D., Fu, P., Wang, Z., Worsnop, D., Jones, R., Percival, C. J., Coe, H., and Sun, Y.: Production of N_2O_5 and $ClNO_2$ in summer in urban Beijing, China, Atmos. Chem. Phys., 18, 11581–11597, https://doi.org/10.5194/acp-18-11581-2018, 2018.